MORPHOGENS

Patterning and growth control in vivo by an engineered GFP gradient

Kristina S. Stapornwongkul[1], Marc de Gennes[1], Luca Cocconi[1,2], Guillaume Salbreux[1]*†, Jean-Paul Vincent[1]*

Morphogen gradients provide positional information during development. To uncover the minimal requirements for morphogen gradient formation, we have engineered a synthetic morphogen in *Drosophila* wing primordia. We show that an inert protein, green fluorescent protein (GFP), can form a detectable diffusion-based gradient in the presence of surface-associated anti-GFP nanobodies, which modulate the gradient by trapping the ligand and limiting leakage from the tissue. We next fused anti-GFP nanobodies to the receptors of Dpp, a natural morphogen, to render them responsive to extracellular GFP. In the presence of these engineered receptors, GFP could replace Dpp to organize patterning and growth in vivo. Concomitant expression of glycosylphosphatidylinositol (GPI)–anchored nonsignaling receptors further improved patterning, to near–wild-type quality. Theoretical arguments suggest that GPI anchorage could be important for these receptors to expand the gradient length scale while at the same time reducing leakage.

During development, morphogens provide positional information by forming long-range concentration gradients. Despite the importance of morphogens, there is still no consensus on how they spread within tissues (*1*). The most parsimonious view is that morphogens travel by diffusion (*1*–*3*). However, epithelia, monolayered sheets of cells, present a particular challenge for diffusion-based mechanisms, as ligand leakage is expected to occur, thus compromising planar gradient formation (*4*) and possibly affecting the development of other tissues and organs (*5*).

Much of our knowledge about the formation and interpretation of morphogen gradients in epithelia comes from studies of the bone morphogenetic protein (BMP) homolog Decapentaplegic (Dpp) in wing imaginal discs of *Drosophila*. In these epithelial pouches, Dpp is produced by a stripe of cells and spreads to form a gradient that organizes growth and patterning along the anterior–posterior (A/P) axis (*6*). It has been suggested that Dpp spreads by planar transcytosis or on specialized filopodia called cytonemes (*7*, *8*). Both mechanisms would ensure planar transport; however, so far, direct functional evidence remains scant. By contrast, there is extensive genetic evidence for the requirement of glypicans in morphogen transport (*9*–*11*). It has been suggested that morphogens can piggyback on laterally diffusing glypicans and pass from cell to cell through cycles of dissociation and reassociation, thus remaining within the plane of the epithelium. Here, we have taken a forward engineering approach to investigate whether an inert protein can form a diffusion-based gradient in the basolateral space of a developing pseudostratified epithelium and specify positional information.

[1]The Francis Crick Institute, 1 Midland Road, London NW1 1AT, UK. [2]Imperial College, Department of Mathematics, London, UK. *Corresponding author. Email: jp.vincent@crick.ac.uk (J.-P.V.); guillaume.salbreux@crick.ac.uk (G.S.)
†Present address: Department of Genetics and Evolution, University of Geneva, Quai Ernest-Ansermet 30, 1205 Geneva, Switzerland.

Extracellular binders reveal a diffusion-based gradient

Synthetic approaches have become a powerful tool to uncover the key features of natural processes (*12*, *13*). To assess the ability of an inert protein to form a gradient in wing imaginal discs of *Drosophila*, we engineered flies to express, from a localized source, green fluorescent protein (GFP) appended with a secretion targeting signal (SecGFP). This was achieved by integrating SecGFP coding DNA into the *patched* (*ptc*) locus (fig. S1), a gene which, like *dpp*, is expressed along the A/P boundary (Fig. 1A). GFP was detectable, albeit weakly, in the expression domain (Fig. 1, B and C, no binders). GFP fluorescence was also present uniformly in the peripodial space, an enclosed lumen on the epithelium's apical side. By contrast, the basolateral space was devoid of detectable GFP, most likely because it is exposed to the larval circulation, which could provide an escape route (fig. S2A). Indeed, GFP can cross the basal lamina to and from the hemolymph (fig. S2), and leakage could therefore prevent locally expressed GFP from forming a detectable gradient in the basolateral space. Natural morphogens, which form gradients, are known to bind various receptors and extracellular components (*11*). We therefore asked whether adding GFP-binding species in the extracellular space would reduce leakage and enable the formation of a detectable gradient in SecGFP-expressing wing imaginal discs.

Extracellular GFP-binding proteins are readily engineered by fusing a transmembrane protein (e.g., human CD8) to one of the many characterized anti-GFP nanobodies (*14*), such as GBP1 (also known as vhhGFP4), which binds GFP with a dissociation constant (K_d) of 0.23 nM (*15*, *16*); we refer to this antibody as Nb1^{high}. DNA encoding this fusion protein (Nb1^{high}CD8) was knocked into the *hedgehog* (*hh*) locus so that it could be expressed at a physiological level in a domain that abuts the *ptc* expression domain (Fig. 1A, gray shading), where SecGFP is produced. In the presence of both genetic modifications, a gradient of GFP fluorescence was readily detectable (Fig. 1, B and C, *hh-Nb1^{high}CD8*) in both the basolateral and apical regions. Here, we focused on the basolateral gradient; a discussion of the apical gradient can be found in fig. S3. The basolateral GFP profile (Fig. 1D, green curve) differed somewhat from a classic exponential, with a shoulder near the source and a nonzero tail far from the source (length scales and nonzero tail values are listed in table S1). Because GFP can diffuse in and out of imaginal discs, we considered the possibility that the nonzero tail could arise from GFP that escaped into the hemolymph (GFP^{hemo}). This was tested by trapping GFP in the hemolymph with Nb1^{high}CD8 expressed at the surface of the fat body, a sprawling organ that lines the body cavity (fig. S2A). In the resulting imaginal discs, the GFP profile decayed all the way to background level, showing that the tail indeed originated from the hemolymph (Fig. 1, C and D, purple curve). In conclusion, a single extracellular binding species reveals the gradient of an inert protein in vivo, but leakage in the hemolymph occurs and interferes with the gradient's shape, most obviously far from the source, at the tail end of the gradient.

Key parameters of gradient formation

Having established that an inert protein can form a gradient in a developing epithelium, we set out to investigate the importance of the surface binders' affinity for GFP. To ask if the high affinity of Nb1 for GFP (0.23 nM) is needed for a detectable gradient to form, this parameter was changed by using, as an extracellular binder, LaG3, which binds GFP with a K_d of 25 nM (*17*); we refer to this protein as Nb^{low}). In imaginal discs carrying *ptc-SecGFP* and *hh-Nb^{low}CD8*, GFP fluorescence was above background but not detectably graded (Fig. 1, C and D, compare blue and black curves;fig. S4 informs a discussion of Nb-mediated GFP fluorescence boosting). This indicated that a low-affinity binder can trap extracellular GFP, but also that sufficiently high affinity is needed for a meaningful gradient of surface-associated GFP to form.

To formalize the role of extracellular binders and leakage in GFP gradient formation, we devised a diffusion–degradation–leakage mathematical model (Fig. 2A and supplementary text), building on previous work (*18*, *19*). Free

Corrected 16 November 2020. See full text.

GFP was assumed to diffuse in the intercellular space with a diffusion constant D and to bind and unbind at rates k_{on} and k_{off} to receptors internalized and degraded at rate k. The flux between hemolymph and the epithelium was assumed to be driven by the concentration difference between them, with a proportionality coefficient κ. At steady state, in the posterior compartment (where the receptors are expressed), the concentrations of free (c) and receptor-bound (n_b) GFP follow these equations:

$$0 = D\partial_x^2 c - \frac{k}{h} n_b - \kappa(c - c_H) \quad (1)$$

$$n_b = n_T \frac{k_{on} c}{k_{off} + k_{on} c + k} \quad (2)$$

where n_T refers to the density of receptors at the cell surface, h is the intercellular distance, and c_H is the free GFP concentration in the hemolymph. Analytical exploration of the model showed that it recapitulated the essential features of the bound GFP gradient profile (Fig. 2B and fig. S5): (i) close to the source, receptor saturation leads to a shoulder; (ii) further away from the source, the profile decays on a length scale determined by the diffusion constant, the degradation of receptors, and leakage to the hemolymph; (iii) far from the source, the concentration of GFP remains at a constant nonzero value that depends on the hemolymph GFP concentration.

We then tested whether the model, and its consideration of leakage in particular, could quantitatively account for observed experimental profiles. To derive the concentration c_H of GFP in the hemolymph, we surmised that it is set by the balance between input from tissue leakage and loss by degradation in the hemolymph (k_H) (supplementary text, where we also discuss the contribution of other larval tissues that produce and degrade the ligand). Parameters were chosen from reasonable estimates or published data, with the remaining unknown parameters obtained from a fit to experimental curves, as described in table S2. Our fitting procedure indicated a substantial leakage rate, κ, of ~1/(13 s). Comparison of Figs. 2C and 1D shows that the model provides a suitable framework to rationalize experimental observations. The effect of reducing affinity was recapitulated by setting this parameter to that measured for Nb^{low} (Fig. 2C, blue curve). Being a poor binder, Nb^{low}CD8 is unable to trap much GFP at the cell surface, reducing the amplitude of the gradient near the source. Consequently, Nb^{low}CD8 takes up and degrades GFP at a relatively low rate, leading to increased leakage (supplementary text, section 1.5). Thus, lowering ligand–binder affinity adversely affects the gradient both by reducing gradient amplitude and by increasing the concentration of GFP in the hemolymph. The model also replicated the effect of the fat body trap by increasing the hemolymph degradation rate ~20-fold (Fig. 2C, purple curve).

The model could also be used for de novo predictions. With the parameters determined above, it predicted that increasing ligand production at the source should lead to gradient extension as well as flattening near the source because of saturation (fig. S6A). This was indeed found experimentally in imaginal discs overexpressing SecGFP under the control of *ptc-Gal4* (fig. S6, B to D). Also confirmed experimentally was the prediction that increasing receptor expression (achieved by boosting the level of Nb1^{high}CD8 ~20-fold, with *hh-Gal4* and *UAS-Nb1^{high}CD8*) (fig. S7A illustrates the quantification) would lead to a steepening of the gradient and an increase in GFP level near the source, although the latter was not as marked in the experiment as in the model (Fig. 3, compare A and C). Both model and experiment showed a reduced nonzero tail in this condition, confirming that receptor-mediated internalization contributes to limiting leakage into the hemolymph. Therefore, increasing ligand–receptor avidity could contribute to reducing the amount of GFP^{hemo} flowing back in the tissue, although this could be at the cost of a reduced range.

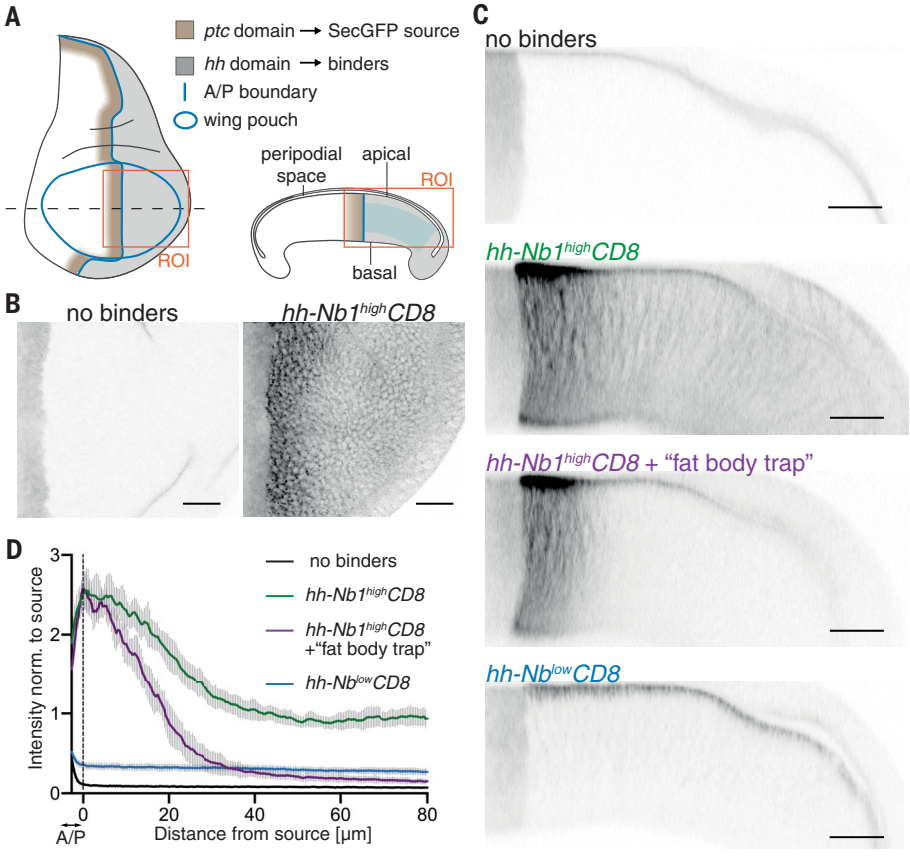

Fig. 1. Establishment of a GFP gradient in a developing epithelium. (**A**) Schematic representation of a wing imaginal disc of *Drosophila*. SecGFP is expressed under the control of the *ptc* promoter (brown), and a membrane-tethered anti-GFP nanobody is expressed under the control of the *hh* promoter (gray). The region of interest (ROI) indicates the areas depicted in (B) and (C). Blue shading indicates the region used to generate the profiles shown in (D). (**B**) In the absence of binders, SecGFP can be seen at the source but is not detectable in basolateral focal planes. Upon expression of high-affinity binders in the posterior compartment (*hh-Nb1^{high}CD8*), a gradient is readily seen. (**C**) Cross sections of imaginal discs expressing SecGFP in the *ptc* domain show that, in the absence of binders, GFP is detectable in the peripodial space but not in the basolateral space. In the presence of binders (*hh-Nb1^{high}CD8*), a gradient can be seen in the basolateral space but with a nonzero tail, which is largely abrogated by concomitant activation of *UAS-Nb1^{high}CD8* in the fat body (+ fat body trap). Only a shallow basolateral gradient is detected when a low-affinity binder is expressed (*hh-Nb^{low}CD8*). (**D**) Fluorescence intensity profiles derived from preparations like those shown in (C). The vertical dotted line marks the estimated posterior edge of the source. The numbers of discs analyzed are as follows: no binders, n = 10; *hh-Nb1^{high}CD8*, n = 11; *hh-Nb1^{high}CD8* + fat body trap, n = 7; *hh-Nb^{low}CD8*, n = 10. Scale bars, 20 µm.

Engineering a GFP-dependent signaling gradient in vivo

In the previous section, we identified minimal conditions for an inert protein to form a gradient along the plane of a developing epithelium. We next asked if this gradient could provide positional information. The best-characterized morphogen in wing imaginal discs is Dpp, which promotes growth and specifies the position of veins along the A/P axis. As a first step toward asking if GFP could substitute for Dpp in vivo, we engineered the Dpp receptors Thickveins (Tkv) and Punt (Put) to render them responsive to GFP. Normally, Dpp dimers bind to two pairs of Tkv and Put, leading to phosphorylation of Mad (*20*) and transcriptional repression of the *brinker* gene (*brk*) (*21*). The resulting inverse Brk gradient in turn controls the nested expression of target genes such as *spalt* (*sal*) and *optomotor-blind* (*omb*) (*22*, *23*) (Fig. 4A). We reasoned that GFP dimers might initiate the same signaling cascade if Tkv and Put were fused to anti-GFP nanobodies [GBP1 (referred to here as $Nb1^{high}$) and GBP6 (here called $Nb2^{high}$)] that recognize nonoverlapping epitopes (*16*, *24*) (fig. S8A). We created plasmids to express $Nb2^{high}$Tkv and $Nb1^{high}$Put and co-transfected them in S2 cells. Addition of GFP dimers (or monomers) to the culture medium led to accumulation of phospho-Mad (pMad), suggesting that the chimeric receptors can be activated by GFP (fig. S8B), although we cannot be sure that the signaling kinetics normally achieved by the natural ligand were entirely recapitulated.

On the basis of these encouraging results with cultured cells, we created a transgene that expresses, in a Flippase (Flp)-dependent manner, both engineered receptors under the control of the *ubiquitin* (*ubi*) promoter (Fig. 4B). This transgene, *ubi-[>STOP>Nb2^{high}Tkv 2A Nb1^{high}Put]*, where > indicates Flp recombination targets, is referred to here as SR (for signaling receptors). We also developed a *dpp* allele that can be inactivated but at the same time be made to express secreted GFP dimers upon Flp expression (*dpp-[>Dpp>SecGFP:GFP]*) (Fig. 4C; validated in fig. S9). First, we used the previously described *dpp-[>Dpp>]* allele (*25*) to confirm that inactivation of *Dpp* throughout the wing primordium with *rotund-Gal4* (*rn-Gal4*) and *UAS-Flp* abrogated growth and patterning, even in the presence of GFP-responsive receptors (Fig. 4D, column 2). Crucially, with *dpp-[>Dpp>SecGFP:GFP]*, which produces GFP upon *Dpp* inactivation, recognizably patterned wings developed (Fig. 4D, column 3). Note that no GFP gradient was detectable in this genetic background, perhaps because of rapid internalization and degradation of GFP by the signaling receptors. The rescuing activity of secreted GFP dimers was further assessed in imaginal discs by staining for various markers of Dpp signaling. pMad immunoreactivity was unexpectedly low in the GFP-producing cells (fig. S10). Most relevant to this study, however, signaling activity was graded on either side of the source, including in the posterior compartment, which relies entirely on ligand diffusion (*26*). In addition, pMad immunoreactivity was also present in a salt-and-pepper manner throughout the whole pouch, as if residual signaling activity persisted far from the source. In agreement, *brk* was repressed over a wider range than in control discs. Both *sal* and *omb* were expressed in GFP-rescued discs, although in a range that did not recapitulate the wild-type situation; in the posterior compartment, the Sal domain boundary was fuzzy, whereas the domain of Omb was too broad. Normally, Sal and Omb ensure the patterned down-regulation of the *Drosophila* serum response factor (DSRF), which is required for vein fate specification (*27*). However, in the "rescue" condition, an oversized domain of DSRF down-regulation could be seen in the posterior compartment, along with a corresponding

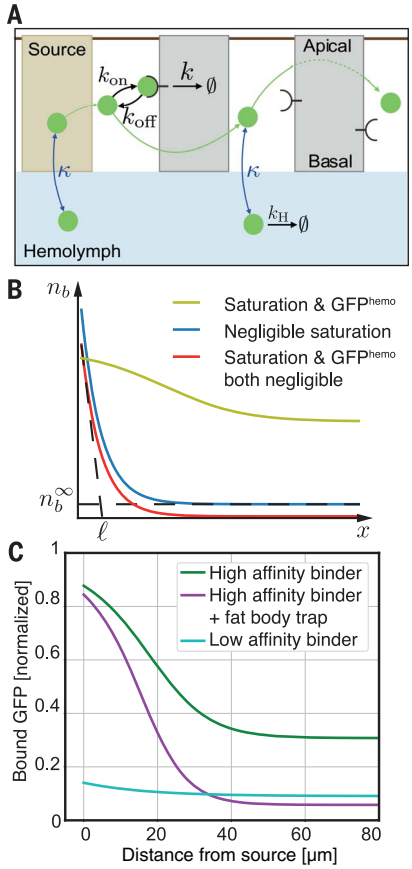

Fig. 2. A diffusion–degradation–leakage model for GFP gradient formation. (**A**) Schematic representation of the model for gradient formation. Parameters are described in the main text and supplementary text. (**B**) Main features of bound GFP profiles predicted by the model using parameters listed in table S2 (unless specified otherwise). The yellow-green curve shows the profile exhibiting receptor saturation near the source and a nonzero tail due to GFP^{hemo} (ligand production rate $j = 0.5$nM/s, $n_T = 100$nM.μm). The blue curve shows that without saturation, the gradient is an exponential with a nonzero tail, $n_b^{\infty} \leq n_T c_H k_{on}/k_{off}$, and a decay length $[l = \sqrt{D/(k_r + \kappa)}]$ that depends on diffusion, effective degradation with rate k_r, and leakage with rate κ ($j = 3{\cdot}10^{-4}$nM/s, $n_T = 3{\cdot}10^{4}$nM.μm). The red curve shows that the ligand concentration set to zero in the hemolymph abolishes the nonzero tail (blue curve with $c_H = 0$). The supplementary text, section 1.3, provides full parameter definitions. (**C**) Bound GFP profiles normalized to the total concentration of receptors. The blue and green curves were obtained with the known on- and off-rates for the low- and high-affinity receptors, respectively. The purple curve was obtained by increasing degradation in the hemolymph. Compare to corresponding experimental curves in Fig. 1D.

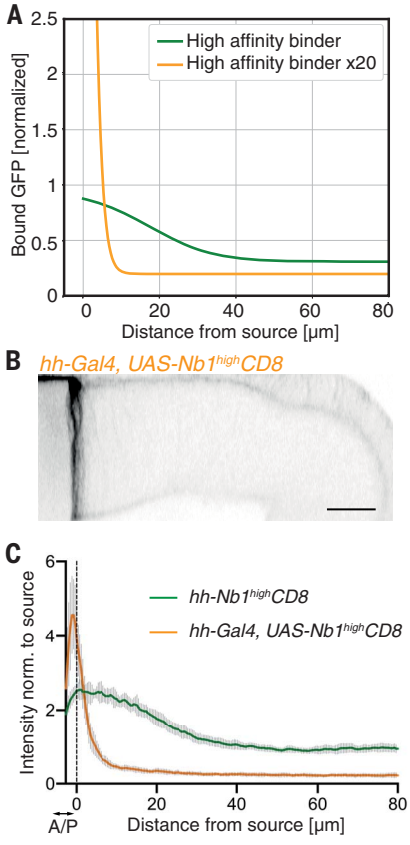

Fig. 3. Predicted and experimental effects of increasing binder expression. (**A**) Predicted GFP profile after a 20-fold increase in binder expression (orange; compare to the green curve, which is reproduced from Fig. 2C). Note the steep gradient and the lower nonzero tail. Bound GFP concentrations are normalized to the lower value of total receptor concentration. (**B**) Cross section of a *ptc-SecGFP* imaginal disc overexpressing the high-affinity binder (*hh-Gal4, UAS-Nb1^{high}CD8*). (**C**) GFP profiles in *hh-Gal4, UAS-Nb1^{high}CD8* (orange curve, $n = 8$), and *hh-Nb1^{high}CD8* discs (green curve from Fig. 1D). Scale bars, 20 μm.

Corrected 16 November 2020. See full text.

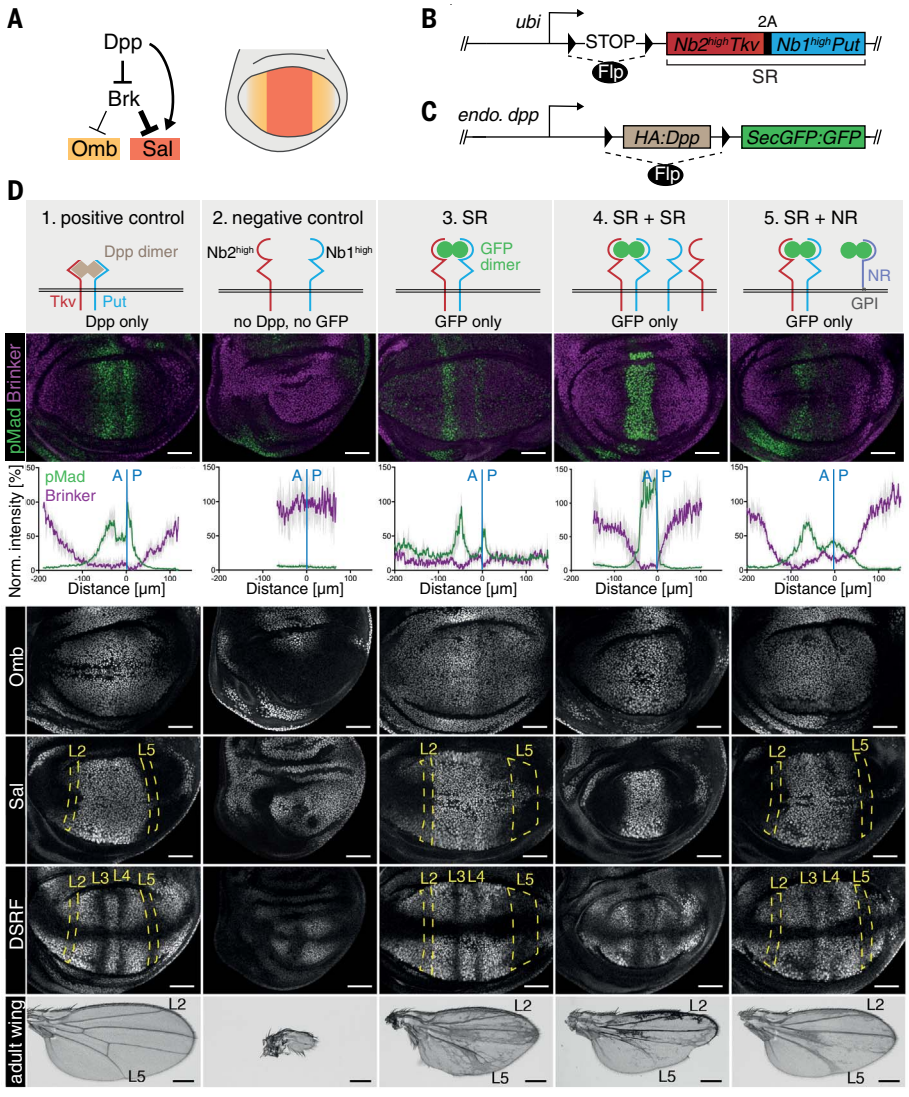

Fig. 4. Rescue of growth and patterning by GFP. (**A**) Target genes of Dpp signaling in the pouch, which give rise to the wing. (**B**) Schematic representation of SR, the transgene for conditional expression of engineered receptors. (**C**) The *dpp* locus engineered to allow Flp-mediated replacement of an essential region by sequences encoding secreted GFP dimers. Throughout the study, *rn-Gal4* and *UAS-Flp* were used to inactivate *Dpp* and/or trigger SR expression specifically in the pouch. (**D**) Phenotypes of wing imaginal discs and adult wings of various genotypes (columns). The positive control (column 1) shows imaginal discs and wings from a *dpp-[>Dpp>SecGFP:GFP]* homozygous larva. Flp is absent and *Dpp* is therefore expressed as in wild-type discs. For the negative control (column 2), we used larvae homozygous for a different conditional allele (*dpp-[>Dpp>]*) (*25*) and carrying the SR transgene. Here, Flp expression inactivates *Dpp* in the pouch without triggering GFP:GFP production while at the same time activating expression of the engineered receptors. The resulting phenotypes recapitulated those of classical *dpp* mutants (e.g., *brk* derepression and growth impairment). Abrogation of Dpp activity shows that the engineered receptors do not trigger signaling in the absence of GFP. If, in combination with the SR transgene, the *dpp-[>Dpp>SecGFP:GFP]* allele is used (column 3, SR), signaling activity (e.g., pMad immunoreactivity near the source) and growth are restored, albeit imperfectly. Note the occasional spots of pMad throughout the pouch, the expanded zone of *brk* repression, the fuzzy boundary of *sal* expression in the posterior compartment, and the disrupted vein pattern. Adding a second SR transgene (column 4, same genotype as in column 3 with one additional SR transgene, SR+SR) led to enhanced pMad at the source and a narrowing of the signaling gradient (relative to SR alone). Addition of non-signaling receptors (column 5, same genotype as in column 3 with addition of *dally-Nb^{low}GPI*, SR+NR) extended the signaling gradient (relative to SR alone). Note the absence of background pMad far from the source and the wild-type–like expression of target genes. Note, however, that vein L4 was often disrupted and vein L5 was slightly broadened in the distal part. Scale bars, 50 µm (for wing discs) or 0.25 mm (for adult wings).

sprawling vein L5 in surviving adult wings. Ectopic vein material was also seen throughout the wings, which was probably a result of global ectopic Dpp signaling. Despite these limitations, the above results suggest that a GFP gradient can stimulate growth and provide substantial patterning information through engineered receptors.

Signaling activity far from the GFP source, e.g., in the form of ectopic pMad, suggests the presence of GFP dimers throughout the disc, perhaps as a result of re-entry from the hemolymph. During our initial analysis of the GFP gradient, we found that leakage could be reduced by increasing the level of extracellular binders (Fig. 3, B and C). We therefore asked if a similar strategy could be used to reduce nonzero tail signaling in rescued discs. Indeed, with two copies of the transgene expressing engineered GFP-responsive receptors (SR + SR), background pMad immunoreactivity was largely abrogated (Fig. 4D, column 4). The target genes *omb* and *sal* were still expressed in a nested fashion; however, the width of these domains, as well as that of the zone of *brk* repression, were narrower than in the wild type (Fig. 4D, compare column 1 with column 4). This suggests that a twofold increase in receptor expression had the beneficial effect of reducing the adverse effect of leakage on signaling activity far from the source, but at the expense of a reduced range. These results can be understood qualitatively in the context of our gradient model (supplementary text section 1.3.2): at low receptor density, receptor activation is too low to trigger target gene activation; at intermediate receptor density, leakage can lead to a high ligand concentration in the hemolymph, triggering signaling and target gene activation far from the source (fig. S5, F and G); at higher receptor density, hemolymph concentration drops but the gradient scale shortens because of increased degradation in the tissue. It appears, therefore, that long-range GFP gradients with low residual signaling far from the source may only be achievable within a narrow range of parameters (fig. S5, F and G).

Beneficial effects of GPI-anchored nonsignaling receptors

The above analysis suggests that, by solely modulating the expression of signaling receptors, it is difficult to reduce leakage without shortening the gradient. Natural morphogens bind not only to signaling receptors but also to nonsignaling extracellular proteins such as glypicans, glycosylphosphatidylinositol (GPI)–anchored heparan sulfate proteoglycans (*11*). We therefore set out to investigate whether low-affinity,

Corrected 16 November 2020. See full text.

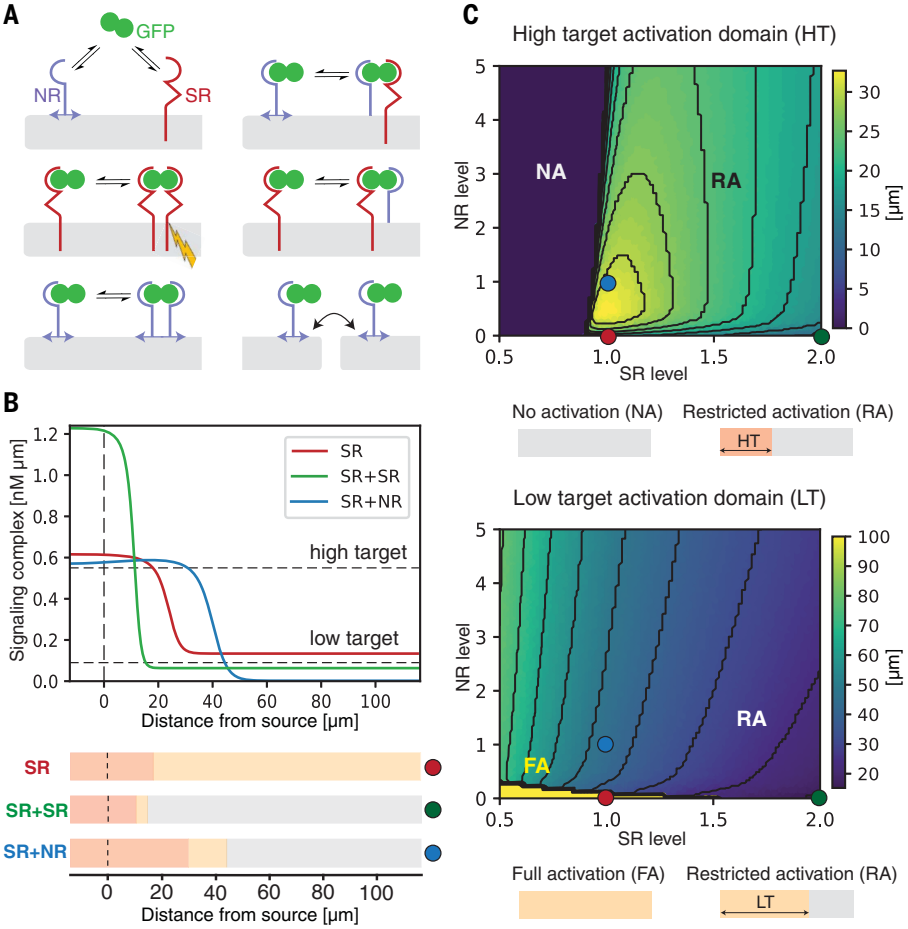

Fig. 5. Modeling the effect of GPI-anchored nonsignaling receptors on a gradient length scale. (**A**) Schematic representation of the molecular interactions considered by our model, including GFP dimer handover and NR hopping. Signal transduction (yellow lightning bolt) is activated by GFP-bound signaling receptor dimers (SR). See supplementary text for details. (**B**) Predicted profiles of signaling complexes in three conditions: a reference case with signaling receptors only (SR; red), doubling SR levels (SR + SR; green), and adding nonsignaling receptors (SR + NR; blue). As observed experimentally, doubling SR leads to a steeper gradient, whereas adding NR reduces GFP^{hemo} signaling and extends the gradient, due to nonsignaling receptor effective diffusion. For illustration, arbitrary thresholds were chosen to indicate the position where high- and low-level target genes would be activated (tables S2 and S3 report the parameter values). (**C**) Width of the high (top) and low (bottom) target activation domains [arbitrary threshold shown in (B)], as a function of normalized levels of SR and NR. Warmer colors indicate a wider target activation domain. Colored dots show parameter combinations used in (B). (Top) For the normalized SR value of 1, increasing NR initially lengthens the high target domain, while a further increase shortens it by preventing access of GFP to SR [as observed experimentally (fig. S11)]. (Bottom) For the normalized SR value of 1 and in the absence of NR, GFP^{hemo} signaling dominates and low target gene is activated throughout (bright yellow region). Increasing SR or NR production both lead to a reduction in the low target domain size.

GPI-anchored, extracellular binders (nonsignaling receptors, NR) would improve the performance of the signaling gradient. As a first step, we created a DNA fragment encoding Nb^{low} [K_d of 25 nM, chosen to mimic the affinity of BMP for heparin (*28*)] tethered to the extracellular face of the plasma membrane by a GPI anchor, Nb^{low}GPI. This fragment was expressed with *rn-Gal4*, which concomitantly triggered expression of Flp to inactivate *Dpp* and initiated expression of SecGFP and the engineered receptors. In the resulting imaginal discs, the signaling activity of SR was suppressed (fig. S11), perhaps because excess Nb^{low}GPI prevented SecGFP from accessing the signaling receptors. To achieve a more reasonable expression level, we inserted the Nb^{low}GPI-encoding fragment in the *dally* locus, one of the two glypican-encoding genes of *Drosophila*. This allele (*dally-Nb^{low}GPI*) was then combined with all the previously described genetic elements needed for a GFP signaling gradient to form. Addition of this nonsignaling receptor extended the pMad gradient and narrowed the domain of *brk* repression, an indication of reduced GFP^{hemo} signaling far from the source (Fig. 4D, compare columns 3 and 5). Indeed, with this combination of signaling and nonsignaling receptors, target gene expression (controlled entirely by GFP dimers) was comparable to that in wild-type imaginal discs, and the resulting wings were notably well patterned, proportioned, and consistently sized (fig. S12).

To rationalize how nonsignaling receptors could improve the signaling gradient's characteristics, we devised a formal description of the relevant molecular interactions (Fig. 5A, fig. S13C, supplementary text and table S3). In this framework, GFP dimers bind signaling and nonsignaling receptors and transit from one configuration to another. Signaling receptors typically undergo rapid endocytosis upon binding to their ligands. By contrast, GPI-anchored binders could have a longer lifetime (*29*), allowing them to hand over ligands to signaling receptors (*30*). Simulations showed, however, that addition of membrane-tethered nonreceptors does not extend the signaling gradient, although they can alter its shape near the source (supplementary text and fig. S13D). We next considered the relevance of the labile nature of GPI anchors (*31*). Locally expressed GFP-GPI spreads within wing imaginal discs (*32*, *33*), suggesting that GPI-anchored proteins can detach from cells and possibly reinsert themselves nearby, a process we call hopping (Fig. 5A). Simulations introducing a tissue-scale effective diffusion constant, $D_r = 0.1\mu m^2/s$, for GFP-Nb^{low}GPI (representing lateral diffusion in the cell membrane and intercellular hopping) can explain the extension of the signaling gradient by Nb^{low}-GPI (Fig. 5B). In fact, we find that, in the absence of NR diffusion (or with a low diffusion constant), NRs can only shorten the gradient, as nondiffusing NRs provide an additional route for ligand degradation without contributing to ligand spread (fig. S13, D and E, and supplementary text). At a high NR concentration, competition for the ligand with SR inhibits signaling (Fig. 5C), as observed experimentally (fig. S11). For intermediate concentrations of the NR, however, NR diffusion enables the gradient range to increase while preventing uniform activation of low-target genes by leaked ligand.

Conclusion

We have shown that, in the presence of extracellular binders, GFP can form a gradient in an epithelial tissue. Because GFP is inert in wing imaginal discs, it is unlikely to spread by a specialized transport mechanism, such as planar transcytosis. The low off-rate of $Nb1^{high}$

(k_{off} = 1.7 × 10^{-4} s^{-1}) also limits the contribution of ligands passing from one receptor to another. We therefore suggest that the GFP gradient forms by free diffusion, even though the readily detectable gradient is largely made up of bound GFP (Fig. 1C and fig. S5, H to K). In the presence of engineered GFP-responsive receptors (SR), diffusing GFP can act as a morphogen. One limitation of free diffusion is that it allows leakage into the circulation, a potential threat to positional information. As we have shown, signaling from leaked GFP can be reduced by increasing the level of SR. However, this was at the expense of a reduced range. Leakage can be reduced without a concomitant decrease in gradient range by adding GPI-anchored nonsignaling receptor (NR). We suggest that, by virtue of their labile association with cell membranes, GPI-anchored nonsignaling receptors can undergo tissue-level diffusion and thus extend the gradient. Although this hypothesis remains to be demonstrated experimentally, our results so far show that a combination of free and NR-assisted diffusion suffices to emulate the range and activity of a natural morphogen.

REFERENCES AND NOTES

1. P. Müller, K. W. Rogers, S. R. Yu, M. Brand, A. F. Schier, *Development* **140**, 1621–1638 (2013).
2. S. Zhou *et al.*, *Curr. Biol.* **22**, 668–675 (2012).
3. S. R. Yu *et al.*, *Nature* **461**, 533–536 (2009).
4. A. D. Lander, Q. Nie, B. Vargas, F. Y. Wan, *J. Mech. Mater. Struct.* **6**, 321–350 (2011).
5. T. B. Kornberg, A. Guha, *Curr. Opin. Genet. Dev.* **17**, 264–271 (2007).
6. M. Affolter, K. Basler, *Nat. Rev. Genet.* **8**, 663–674 (2007).
7. E. V. Entchev, A. Schwabedissen, M. González-Gaitán, *Cell* **103**, 981–992 (2000).
8. S. Roy, H. Huang, S. Liu, T. B. Kornberg, *Science* **343**, 1244624–1244624 (2014).
9. U. Häcker, K. Nybakken, N. Perrimon, *Nat. Rev. Mol. Cell Biol.* **6**, 530–541 (2005).
10. H. Nakato, J. P. Li, *Int. Rev. Cell Mol. Biol.* **325**, 275–293 (2016).
11. D. Yan, X. Lin, *Cold Spring Harb. Perspect. Biol.* **1**, a002493–a002493 (2009).
12. P. Li *et al.*, *Science* **360**, 543–548 (2018).
13. S. Toda *et al.*, *Science* **370**, 327–331 (2020).
14. S. Harmansa, I. Alborelli, D. Bieli, E. Caussinus, M. Affolter, *eLife* **6**, e22549 (2017).
15. U. Rothbauer *et al.*, *Nat. Methods* **3**, 887–889 (2006).
16. A. Kirchhofer *et al.*, *Nat. Struct. Mol. Biol.* **17**, 133–138 (2010).
17. P. C. Fridy *et al.*, *Nat. Methods* **11**, 1253–1260 (2014).
18. A. D. Lander, Q. Nie, F. Y. M. Wan, *Dev. Cell* **2**, 785–796 (2002).
19. T. Bollenbach, K. Kruse, P. Pantazis, M. González-Gaitán, F. Jülicher, *Phys. Rev. E Stat. Nonlin. Soft Matter Phys.* **75**, 011901 (2007).
20. S. J. Newfeld *et al.*, *Development* **124**, 3167–3176 (1997).
21. B. Müller, B. Hartmann, G. Pyrowolakis, M. Affolter, K. Basler, *Cell* **113**, 221–233 (2003).
22. R. Barrio, J. F. de Celis, *Proc. Natl. Acad. Sci. U.S.A.* **101**, 6021–6026 (2004).
23. R. Sivasankaran, M. A. Vigano, B. Müller, M. Affolter, K. Basler, *EMBO J.* **19**, 6162–6172 (2000).
24. J. C. Tang *et al.*, *Cell* **154**, 928–939 (2013).
25. P. S. Bosch, R. Ziukaite, C. Alexandre, K. Basler, J.-P. Vincent, *eLife* **6**, e22546 (2017).
26. C. J. Evans *et al.*, *Nat. Methods* **6**, 603–605 (2009).
27. J. F. De Celis, *BioEssays* **25**, 443–451 (2003).
28. R. Ruppert, E. Hoffmann, W. Sebald, *Eur. J. Biochem.* **237**, 295–302 (1996).
29. S. Mayor, H. Riezman, *Nat. Rev. Mol. Cell Biol.* **5**, 110–120 (2004).
30. J. Schlessinger, I. Lax, M. Lemmon, *Cell* **83**, 357–360 (1995).
31. G. A. Müller, *Arch. Biochem. Biophys.* **656**, 1–18 (2018).
32. V. Greco, M. Hannus, S. Eaton, *Cell* **106**, 633–645 (2001).
33. C. Tempesta, A. Hijazi, B. Moussian, F. Roch, *PLOS ONE* **12**, e0185897 (2017).

ACKNOWLEDGMENTS

We thank C. Alexandre for generating *vg-Gal4* and *dally-attP* and advice on genome engineering and the Crick Fly Facility for DNA injections. We also acknowledge the technical and intellectual contributions of S. Crossman and I. McGough. J. Briscoe provided comments on the manuscript. We are also grateful to A. Lander for pointing out the possible relevance of GPI's loose anchorage to membranes. We thank H. Ashe, G. Pflugfelder, and A. Salzberg for the generous gift of antibodies. The Developmental Studies Hybridoma Bank also provided antibodies. Drosophila stocks obtained from the Bloomington Drosophila Stock Center (NIH P40OD018537) were used in this study. **Funding:** This work was supported by core funding from the Francis Crick Institute (FC001204 to J.-P.V. and FC001317 to G.S.) and a Wellcome Trust Investigator Award to J.-P.V. (206341/Z/17/Z). K.S.S. was the recipient of a PhD Studentship from the Wellcome Trust (109054/Z/15/Z). **Author contributions:** This project was conceived by K.S.S., J.-P.V., and G.S. K.S.S. designed and performed all the experiments. The results were analyzed by all authors. S. H. Crossman contributed to project design and tool validation. The model was conceived by G.S., M.d.G., and L.C., and numerical simulations were performed by M.d.G. and L.C. The main text was written by K.S.S., J.-P.V., and G.S. with comments from M.d.G. and L.C. **Competing interests:** The authors declare no competing or financial interests. All data are described in the main text or supplementary materials. **Data and materials availability:** All materials are available upon request. A link to the computer code can be found in the supplementary text.

SUPPLEMENTARY MATERIALS

science.sciencemag.org/content/370/6514/321/suppl/DC1
Materials and Methods
Supplementary Text
Figs. S1 to S13
Tables S1 to S3
References (*34*–*61*)
MDAR Reproducibility Checklist

View/request a protocol for this paper from *Bio-protocol*.

21 March 2020; accepted 21 August 2020
10.1126/science.abb8205

Patterning and growth control in vivo by an engineered GFP gradient

Kristina S. Stapornwongkul, Marc de Gennes, Luca Cocconi, Guillaume Salbreux, and Jean-Paul Vincent

Science, **370** (6514), .
DOI: 10.1126/science.abb8205

Engineering synthetic morphogens

Morphogens provide positional information during tissue development. For this behavior to occur, morphogens must spread out and form a concentration gradient; however, their mechanism of transport remains a matter of debate. Stapornwongkul *et al.* now show that in the presence of extracellular binding elements (binders), the inert green fluorescent protein (GFP) can form a detectable concentration gradient by diffusion in the developing fly wing (see the Perspective by Barkai and Shilo). When combining the expression of nonsignaling binders and receptors engineered to respond to GFP, a synthetic GFP gradient can substitute for a natural morphogen to organize growth and patterning. In related work, Toda *et al.* also show that GFP can be converted into a morphogen by providing anchoring interactions that tether the molecule, forming a gradient that can be recognized by synthetic receptors that activate gene expression. These synthetic morphogens can be used to program de novo multidomain tissue patterns. These results highlight core mechanisms of morphogen signaling and patterning and provide ways to program spatial tissue organization independently from endogenous morphogen pathways.

Science, this issue p. 321, p. 327; see also p. 292